Supplementary figures

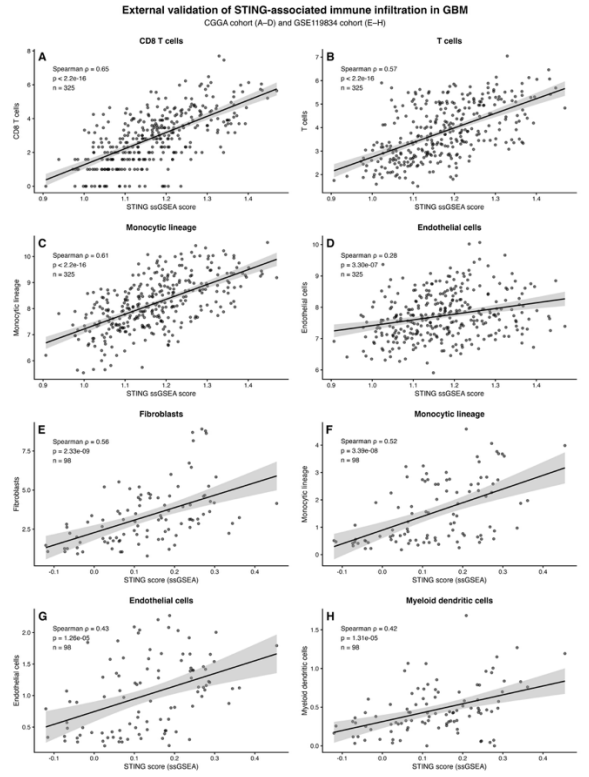

Supplementary Figure S1. External validation of STING-associated immune infiltration across independent glioblastoma cohorts.
(A–D) Correlation analyses between STING pathway activity (ssGSEA score) and immune or stromal cell populations in the CGGA cohort. Increased STING pathway activity was positively associated with CD8 T cells, T cells, monocytic lineage, and endothelial cells.
(E–H) Validation analyses in the independent GSE119834 cohort demonstrating consistent positive associations between STING pathway activity and tumor microenvironmental signatures, including fibroblasts, monocytic lineage, endothelial cells, and myeloid dendritic cells.

Spearman correlation coefficients and p values are shown within each panel. Solid lines represent linear regression fits with shaded 95% confidence intervals. All analyses were performed using MCP-counter-derived cell population estimates.

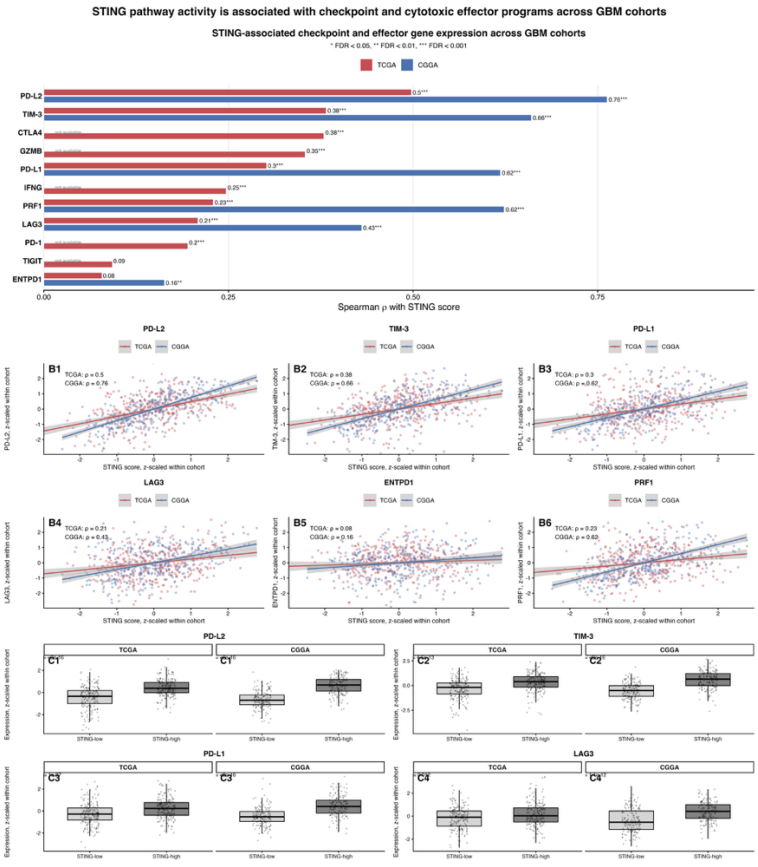

Supplementary figure S2. Cross-cohort validation of STING-associated immune checkpoint and cytotoxic effector programs in GBM.
(A) Spearman correlation analysis demonstrating associations between STING pathway activity and immune checkpoint or cytotoxic effector genes across TCGA and CGGA GBM cohorts. Bars represent Spearman correlation coefficients (ρ). Red indicates TCGA and blue indicates CGGA. Asterisks denote FDR-adjusted significance (* FDR < 0.05, ** FDR < 0.01, *** FDR < 0.001). Genes unavailable in a given cohort are indicated accordingly.

(B1–B6) Representative scatterplots showing cohort-specific associations between STING pathway activity and selected checkpoint or effector genes (PD-L2, TIM-3, PD-L1, LAG3, ENTPD1, and PRF1). Expression values and STING scores were z-scaled within each cohort for visualization. Lines represent linear regression fits with shaded 95% confidence intervals.

(C1–C4) Boxplots comparing expression of representative checkpoint genes between STING-low and STING-high tumors in TCGA and CGGA cohorts. Expression values were z-scaled within cohort. STING-high and STING-low groups were defined using median STING pathway scores. Collectively, these analyses demonstrate reproducible associations between STING pathway activity and immune checkpoint/cytotoxic programs across independent GBM datasets.

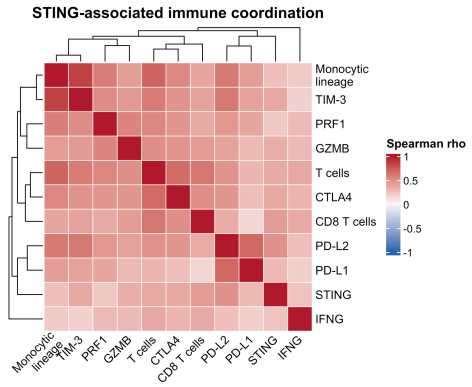

Supplementary Figure S3. Pairwise correlation analysis of STING pathway activity and immune-associated transcriptional programs in GBM.
Heatmap showing Spearman correlation coefficients among STING pathway activity, immune infiltration signatures, cytotoxic effector genes, and immune checkpoint markers in TCGA glioblastoma samples. Hierarchical clustering demonstrates broadly positive associations across immune-related features, with coordinated clustering of cytotoxic and checkpoint-associated transcriptional programs.

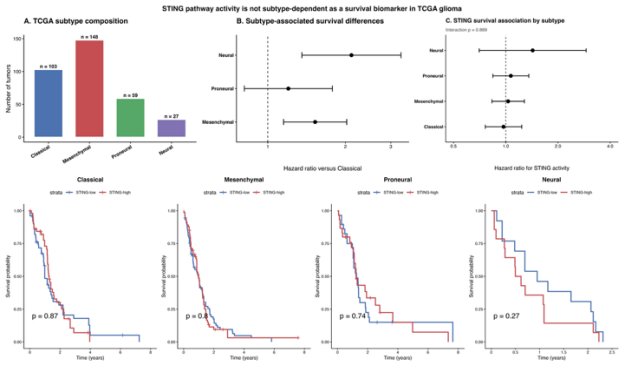

Supplementary Figure S4. Subtype-specific survival analyses of STING pathway activity in TCGA GBM.
(A) Distribution of transcriptomic subtypes in the TCGA GBM cohort after integration of Verhaak molecular subtype annotations. Mesenchymal tumors represented the largest subgroup, followed by Classical, Proneural, and Neural tumors.
(B) Forest plot showing subtype-associated hazard ratios relative to the Classical subtype from the multivariable Cox proportional hazards model adjusted for age and STING pathway activity. Mesenchymal and Neural subtypes were associated with significantly worse overall survival compared with Classical tumors.

(C) Forest plot demonstrating subtype-specific associations between STING pathway activity and overall survival. Hazard ratios for STING pathway activity were estimated separately within each subtype using age-adjusted Cox proportional hazards models. No subtype demonstrated a statistically significant survival association with STING pathway activity. The STING-by-subtype interaction likelihood-ratio test was not significant (LRT p = 0.889), indicating no evidence that the prognostic effect of STING pathway activity differed across transcriptomic subtypes.
(D) Kaplan–Meier survival curves stratified by STING-high versus STING-low tumors within each subtype. Median-based dichotomization of STING pathway activity was performed separately within each subtype. No significant survival differences were observed between STING-high and STING-low tumors in any subtype.

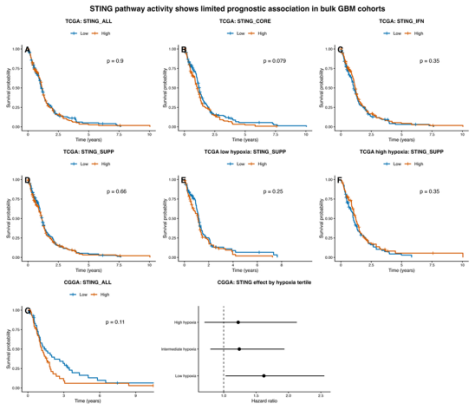

Supplementary Figure S5. STING pathway activity shows limited prognostic association in bulk GBM cohorts.

Kaplan–Meier analyses of overall survival stratified by median STING pathway activity scores across TCGA and CGGA glioblastoma cohorts.
(A–D) TCGA survival analyses for STING_ALL, STING_CORE, STING_IFN, and STING_SUPP modules.
(E–F) TCGA STING_SUPP survival analyses stratified by hypoxia status, where hypoxia groups were dichotomized using the median HYPOXIA score.
(G) CGGA overall survival analysis for STING_ALL.
(H) Age-adjusted Cox proportional hazards models evaluating the association between STING pathway activity and survival across CGGA hypoxia tertiles. Hazard ratios and 95% confidence intervals are shown.

All p-values were calculated using the log-rank test (Kaplan–Meier panels) or Wald test (Cox models). Time is shown in years. Kaplan–Meier analyses using median-based dichotomization were performed for visualization purposes only.

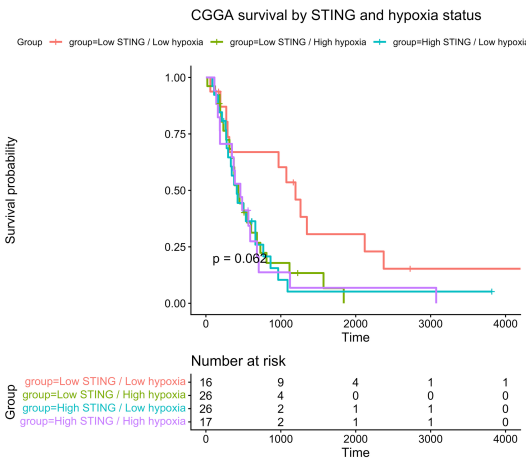

Supplementary Figure S6. Kaplan–Meier analysis of overall survival stratified by combined STING pathway activity and hypoxia status in the CGGA GBM cohort.

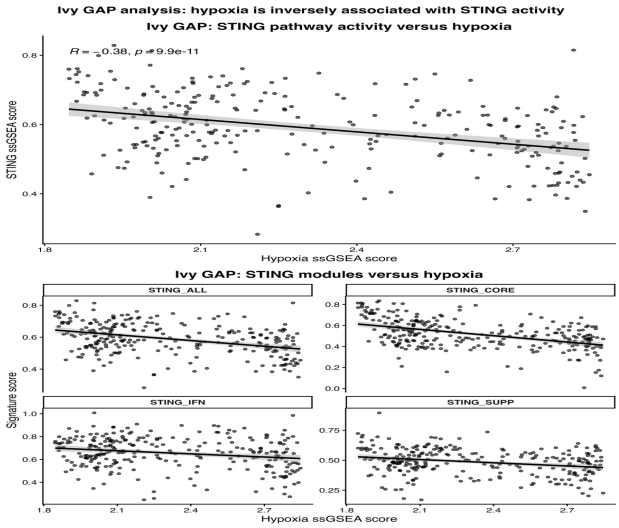

Supplementary Figure S7. Association between hypoxia and STING pathway / modules activity in Ivy GAP samples.
STING pathway scores and hypoxia ssGSEA scores were computed for Ivy GAP samples. The upper panel shows the association between hypoxia and the composite STING_ALL score. Lower panels show associations between hypoxia and individual STING modules, including STING_ALL, STING_CORE, STING_IFN, and STING_SUPP. Points represent individual Ivy

GAP samples. Solid lines indicate linear regression fits with shaded 95% confidence intervals.

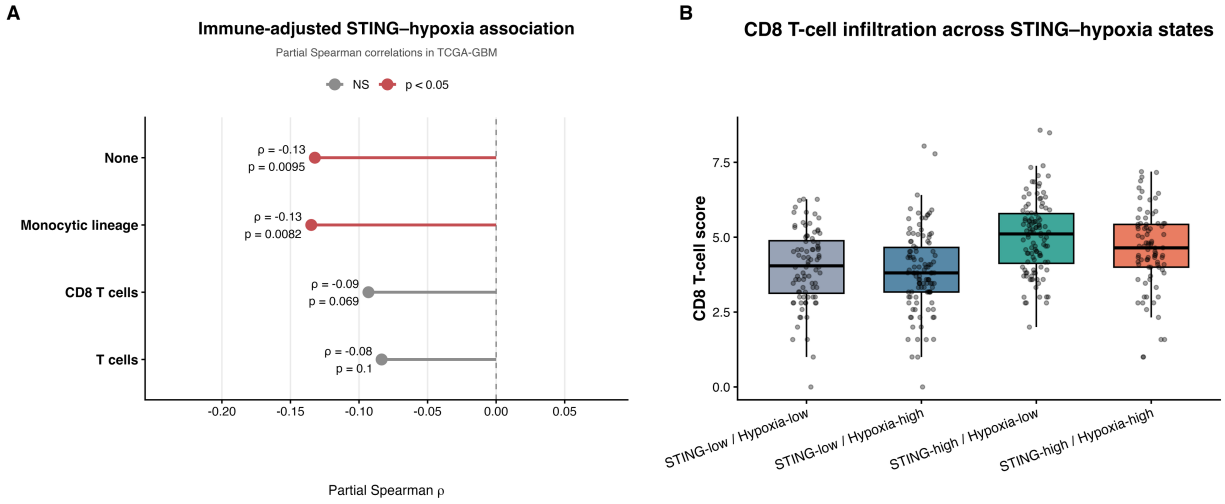

Supplementary Figure S8. Immune context of the STING–hypoxia relationship in TCGA-GBM.
(A) Partial Spearman correlation analyses evaluating the association between STING pathway activity and hypoxia after adjustment for immune cell infiltration signatures. The inverse STING–hypoxia association remained significant after adjustment for monocytic lineage infiltration, but was attenuated after adjustment for CD8 T-cell or total T-cell signatures. (B) CD8 T-cell infiltration scores stratified by combined STING and hypoxia states. Tumors with high STING activity demonstrated higher CD8 T-cell infiltration irrespective of hypoxia status.